Automated on-chip rapid microscopy, phenotyping and sorting of *C. elegans*

Kwanghun Chung, Matthew M Crane & Hang Lu

Supplementary figures and text:

Supplementary Figure 1 Features of the engineered microchip.

Supplementary Figure 2 Mechanism of worm loading.

Supplementary Figure 3 Temperature profile inside the device.

Supplementary Figure 4 YFP::RAB-5 patterns in immobilized worms.

Supplementary Figure 5 Classification features.

Supplementary Figure 6 In-line coarse filtering device.

Supplementary Figure 7 Manual classification of strain CX6858.

Supplementary Methods

Note: Supplementary Videos 1–8 are available on the Nature Methods website.

Supplementary Figure 1 Features of the engineered microchip.

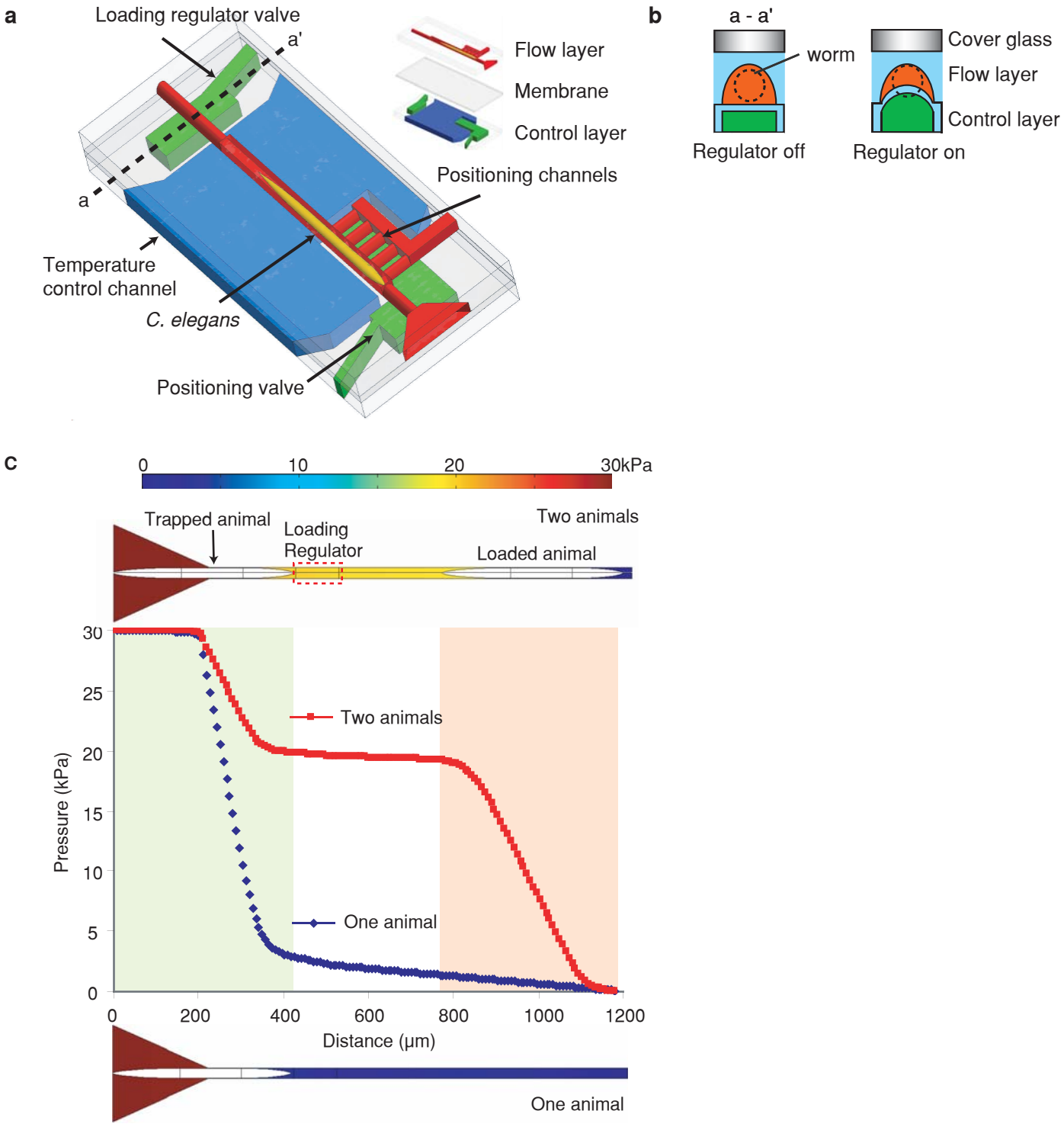

Supplementary Figure 1. Features of the engineered microchip. (**a**) Artist's rendering of the detection zone of the microchip showing device layers in 3-D. Inset: exploded view of the schematic illustration showing the individual layers. (**b**) Schematics of cross-sectional view (a-a') of the self-regulated sample-loading valve shown in (**a**). (**c**) Pressure profile in the imaging chamber determined by 3-D numerical simulation in COMSOL. Top: top view of a two-animal model, showing pressure profile for a loaded animal in the imaging zone and a second animal waiting behind the loading-regulator. Middle: Line plot of the pressure profiles. Bottom: top view of a one-animal model, showing pressure profile for a single animal behind the loading regulator (and no animal in the imaging zone).

Supplementary Figure 2 Mechanism of worm positioning.

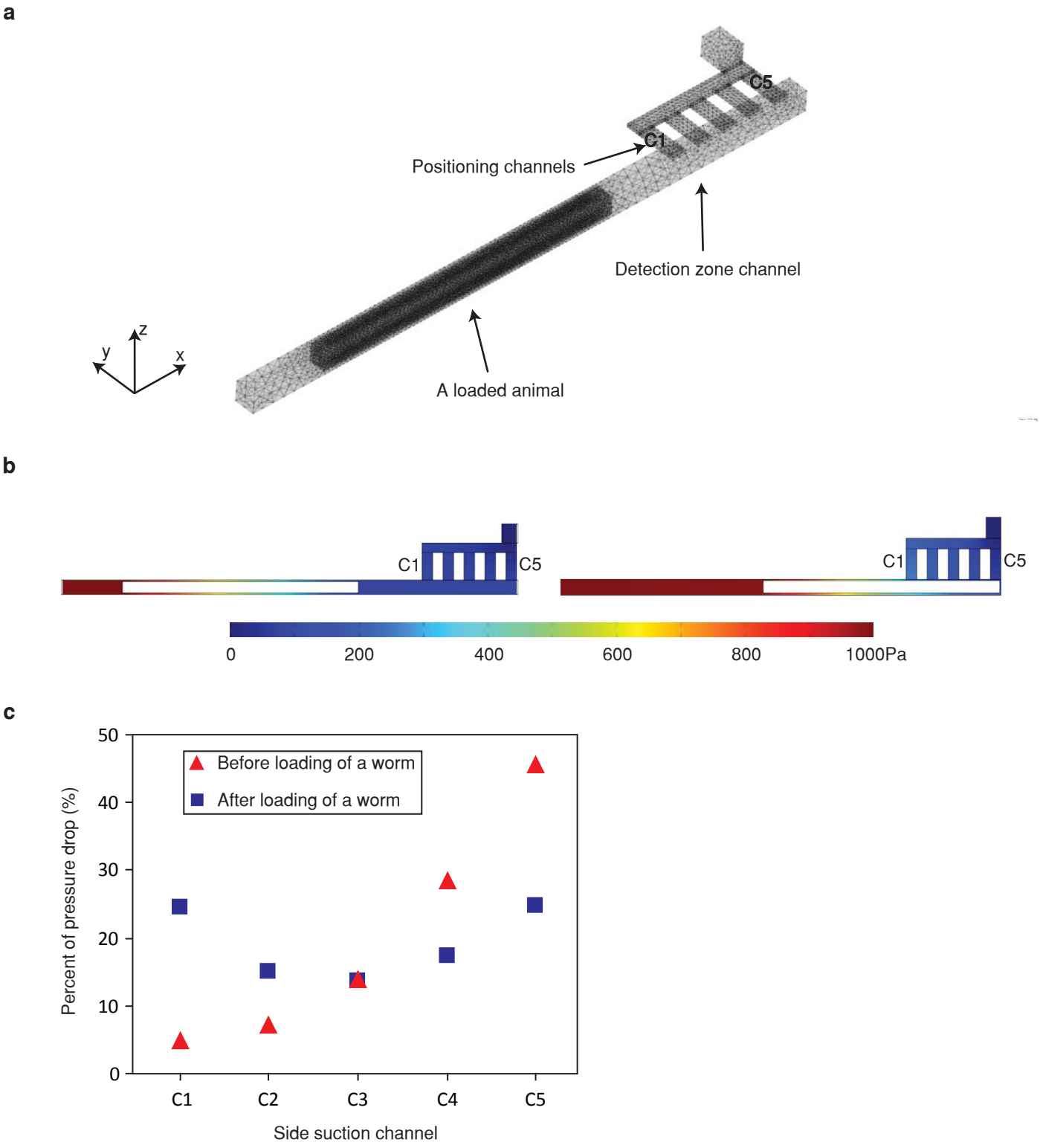

Supplementary Figure 2. Mechanism of worm positioning. Pressure drop distribution along the positioning channels before and after a worm is loaded, determined by numerical simulations. (a) Geometry of the channels and finite element mesh used in numerical simulations. To simplify the numerical simulations, a worm in the channel is assumed as a rectangular rod with 24 μm width and 500 μm length. The height of partially closed side suction channels is assumed as 5 μm. The width and height of the detection zone are 30 μm. Each positioning channel is labeled as C1-C5 from the left respectively. (b) Pressure profile at the vertical middle plane of the side suction channel (2.5 μm from the bottom of the channel) before (Left) and After (Right) a worm is loaded. (c) Plot of the fraction of pressure drop along each positioning channel before (triangle) and after (square) an animal is loaded.

Supplementary Figure 3 Temperature profile inside device.

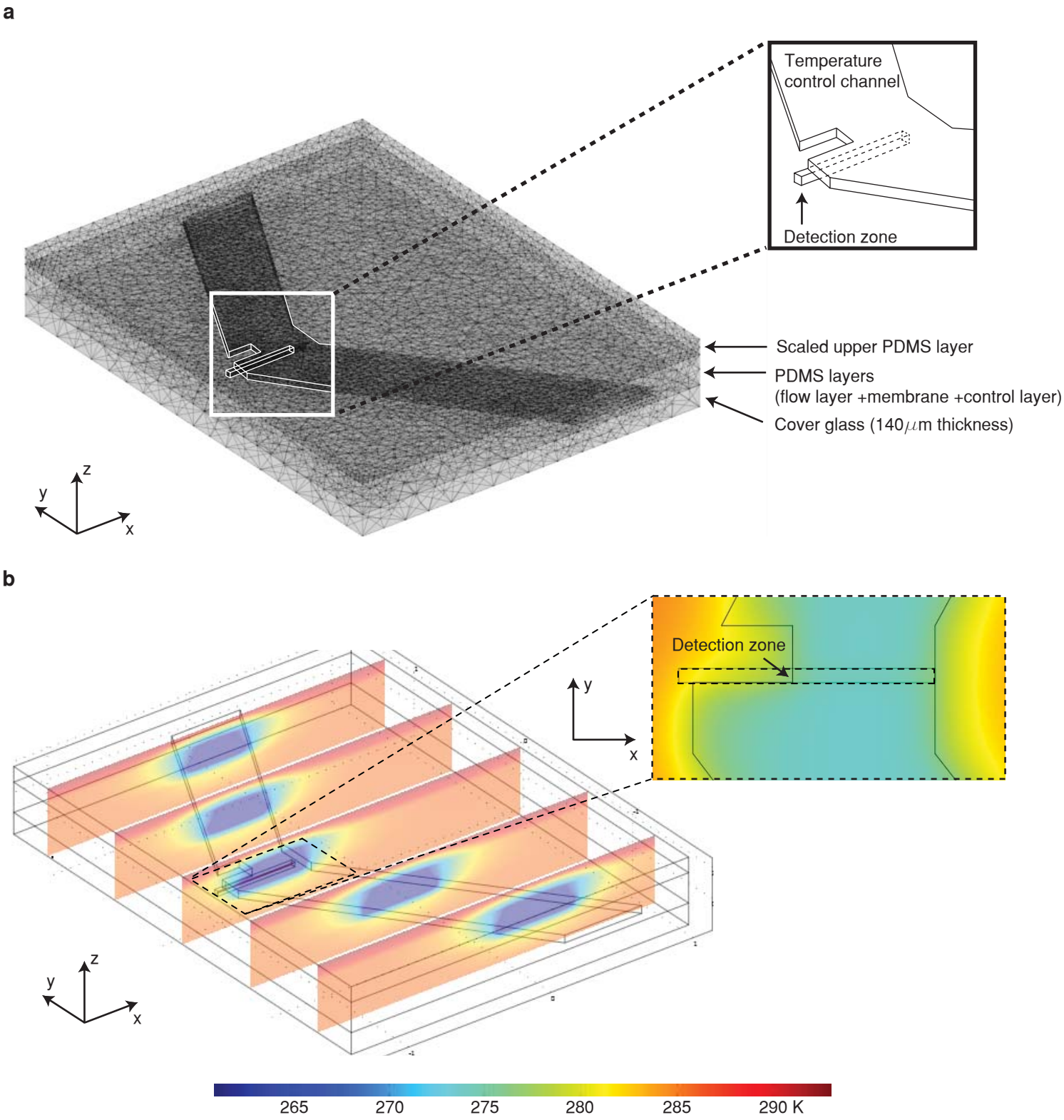

Supplementary Figure 3. Temperature profile inside device. Temperature profiles determined by numerical simulations using physical parameters and experimentally measured boundary conditions. (a) Geometry of the device and finite element mesh used in numerical simulation. Inset: zoom-in view showing the outline of the temperature control channel and detection zone. (b) Temperature profile at the various cross-section of the device showing local cooling. Inset: temperature profile at the vertical mid-plane of the detection zone.

Supplementary Figure 4 YFP::RAB-5 distribution in immobilized worms.

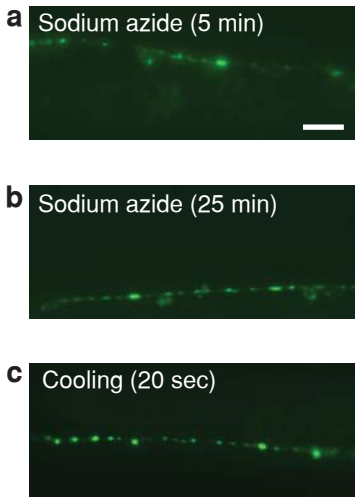

Supplementary Figure 4. YFP::RAB-5 patterns in immobilized worms. Representative images of YFP::RAB-5 distribution in *unc-16*$^{-/-}$ mutant immobilized with either (**a**,**b**) 10 mM of sodium azide or (**c**) cooling, showing similar punctal patterns. Scale bar: 10 μm.

Supplementary Figure 5 Classification features.

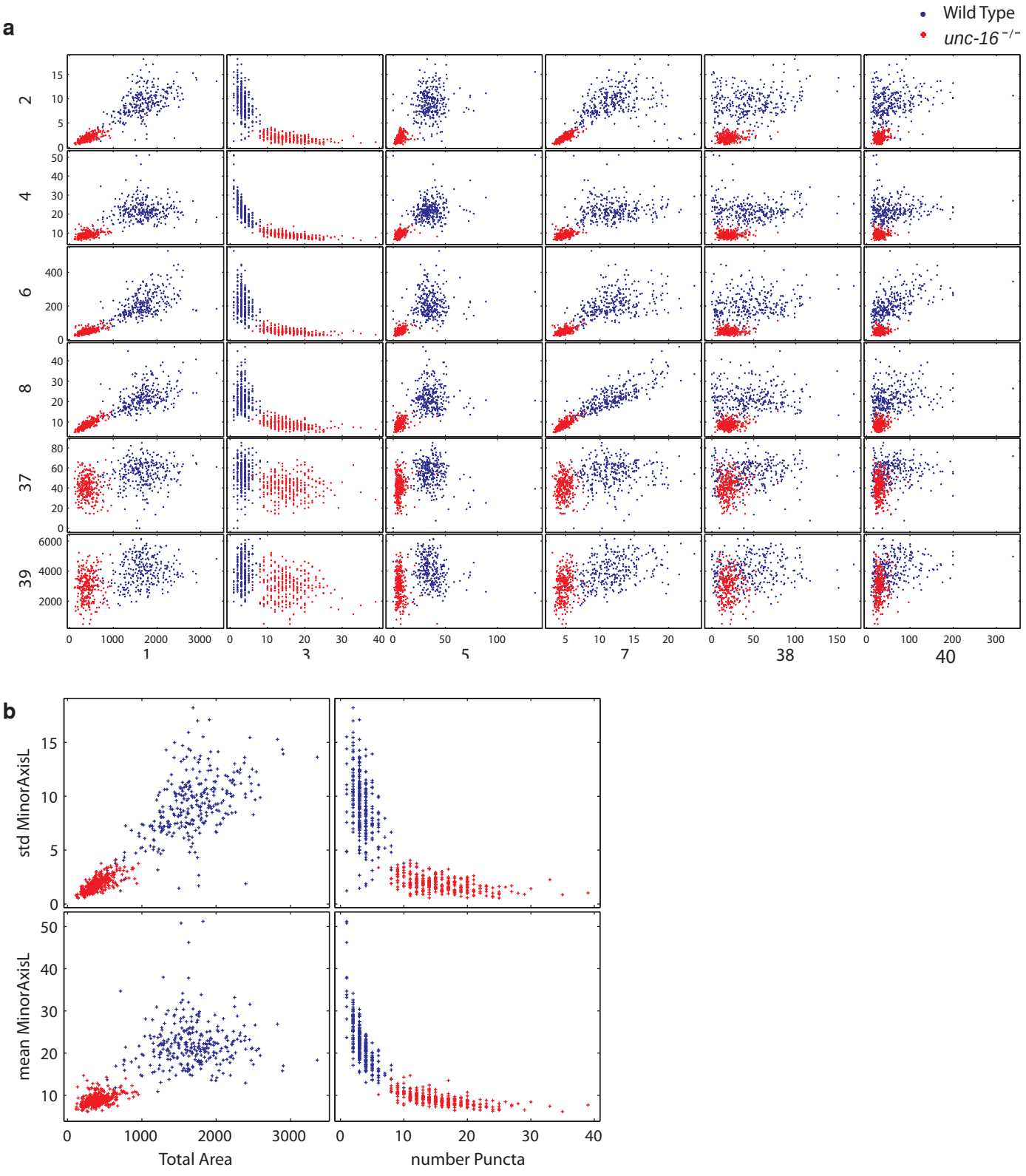

Supplementary Figure 5. Classification features. Graphs showing the distribution of a variety of features used to classify animals as either wild-type or mutant. (a) A variety of selected features that show different degrees of distribution and efficacy in discriminating between classes. Features 2, 4, 6, 8, 37, 39 correspond to std of minor axis length, mean of minor axis length, std major axis length, mean orientation, mean ellipticity. Features 1, 3, 5, 7, 38, 40 correspond to total area, number of puncta, mean area, std of area, std orientation and std ellipticity. (b) A few morphological features responsible for most of the differences between *unc-16*$^{-/-}$ and wild-type classes.

Supplementary Figure 6 In-line coarse filtering device.

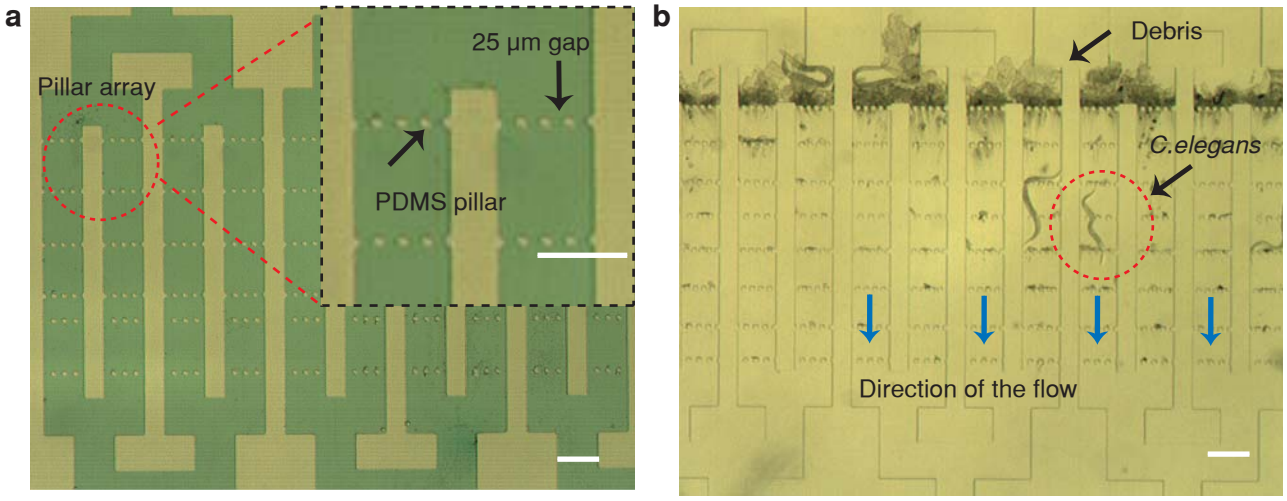

Supplementary Figure 6. In-line coarse filtering device. (**a**) Optical micrograph of the filtering device: channels filled with a green dye solution. Inset: zoom-in view of the channel with PDMS pillar array. (**b**) Debris aggregated in the filtering device. Worms are able to pass through the pillar array. Scale bar: 200 μm.

Supplementary Figure 7 Manual classification of strain CX6858.

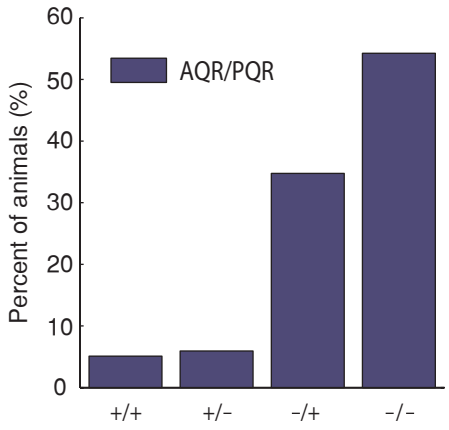

Supplementary Figure 7. Manual classification of strain CX6858. Percentage of animals with each of the four possible expression patterns of GFP in AQR and PQR, n = 118. This figure compares very closely to the automated imaging performed by the system (**Fig. 3n**). Our automated system, however, has throughput of hundreds of animals per hour as compared to manual imaging of tens of animals per hour.

Suppplementary Methods

1. Microfluidic device operation

An automated operation cycle of the microchip is demonstrated in **Figure 2a-d** and **Supplementary Video 1**. This automated phenotyping and sorting process is gentle, and in our experiments, ~100% of animals were viable, crawling on agar and thrashing in buffer normally immediately after the processing.

To load an animal into the imaging chamber, both outlet channels are closed while the side positioning channels remain open (**Fig. 2a** and **Supplementary Video 1** online), and a constant pressure source is used to drive the flow into the microchip. Self-regulation of loading (one animal at a time into the imaging chamber) is critical for high-resolution imaging and accurate sorting. When an animal is present in the imaging chamber, the flow resistance is increased. The reduced flow rate lowers the pressure on a second animal at the sample-loading regulator located at the entrance of the imaging chamber to a point where it is not sufficient to push the second animal into the chamber (**Supplementary Fig. 1** and **Supplementary Video 2** online). Upon releasing the first animal (by opening one of the exit valves), the pressure drop across the second animal becomes sufficient to push it into the imaging chamber. We implemented the sample-loading regulator design by controlling the pressure on a partially closed valve. We thus achieve great flexibility depending on the size of the animals for each application because of our ability to fine-tune the system pressure (5-10 psi) as well as the sample-loading regulator pressure (10-20 psi).

To position the animal precisely and reproducibly inside the imaging chamber, we make use of pressure differences between the positioning channels and the entrance of the main channel (**Supplementary Fig. 2** online). The height of the positioning channels is also controlled by the partially closed positioning valve, similar to the loading regulator valve. Once the animal's nose or tail is positioned at the end of the detection zone, the hydrodynamic resistance of the positioning channels self-equalizes and thereby the pressure force is distributed. This distribution of the pressure force prevents the animal from being forced through the positioning channel and minimizes mechanical stress on the animal.

2. Microfluidic device fabrication

The microfluidic device was fabricated using multi-layer soft lithography. Two different molds were first fabricated by photolithographic processes to create worm loading layer and the control layer. The mold for the worm loading layer was made by a two-step photolithographic process. In the first step, a 30-μm-thick negative photoresist (SU8-2025, Microchem) was spin-coated onto a silicon wafer for the worm loading chamber and the detection channel. The loading regulator, side channels, and outlets were then fabricated with a 25-μm layer of positive photoresist (AZ 50XT, AZ Electronic Materials) on the same wafer. After the positive photoresist was developed, the wafer was heated at 125 ºC for 5 min to allow the positive photoresist to reflow so that the channels form a smooth and rounded shape. The master for the control layer was made of a 50-μm layer of negative photoresist (SU8-2050, Microchem) on a silicon wafer. The

two molds and a blank wafer were treated with tridecafluoro-1,1,2,2-tetrahydrooctyl-1-trichlorosilane vapor (United Chemical Technologies) in a vacuum desiccator to prevent adhesion of PDMS during the molding process.

For fabricating the control layer polydimethylsiloxane (PDMS, Sylgard 184, Dow Corning A and B in 5:1 ratio) was poured onto the control-layer master to obtain a 5 mm-thick layer. Mixture of PDMS (A and B in 20:1 ratio) and THF in 2:1 ratio was spin-coated on a blank wafer to give a 20 μm-thick layer. Both were partially cured at 70 ºC for 20 min. The thick control layer was then peeled off from the master and holes were punched for access to the control and cooling channels. The control layer was then bonded to the thin PDMS membrane on the blank wafer. This assembled control layer was fully cured at 70 ºC for 2 hours. For the worm-loading layer PDMS was spin-coated onto the master to give a 60 μm-thick layer. The worm-loading layer was fully cured in a convection oven at 70 ºC for 2 hours and then was peeled off from the master[1]. The layer was then turned upside down and bonded to the control layer using oxygen plasma treatment. Another set of holes were punched for access to the worm loading channel. These assembled layers were then bonded onto the cover glass to form the micro device.

3. *C. elegans* culture and sample preparation

Animals were cultured according to established methods[2]. Age-synchronized L4 worms were prepared as follows: eggs were obtained by bleaching adults using a solution containing about 1% NaOCl and 0.1 M NaOH, washed and let hatch in M9 buffer, and cultured on Nematode Growth Medium (NGM) plates seeded with *E. coli* OP50. Animals were washed and suspended in M9 solution containing 0.5 wt% Bovine Serum Albumin (BSA) for each experiment.

4. Equipment

The equipment utilized during our experiments includes the following:

- Peltier cooler: PJT-5 30mm square and PJT-6 40 mm square peltier coolers.
- Aluminum tubing: Aluminum alloy 3003 tubing with .0345” ID and .063” OD.
- Digital I/O Card: USB 6501 digital I/O card purchased from National Instruments.
- Solenoid Valves: Solenoid valves from Hargraves Fluidics.
- Valve Manifold: Custom designed.
- Air Pressure Manifold: Custom designed.
- Amplifier Card: Custom designed to amplify signal from the 6501 I/O card.
- Microscope: Leica DM4500.
- Camera: Hamamatsu C9100-13 EM CCD.
- Light Source: Mercury arc lamp.
- Lenses: 10X NA = 0.3, 100X NA = 1.4.

5. Filtering device fabrication

To get rid of dust particles and debris in the worm suspension, a filtering device was fabricated using single-mold soft lithography. The device consists of 40-μm thick channels with a pillar array ~25-30 μm apart. Worms can deform to pass through the gap between pillars, but debris bigger than the gap are filtered out (**Supplementary Fig. 6**).

6. System Control, Image Acquisition, and Image Processing

The code for the worm sorting contains three basic elements: waiting for a worm to enter the detection zone, grabbing images and performing the image processing, and allowing the worm to exit before returning to the initial state. Most image acquisition, even at 100x, requires only a few seconds. An exposure time of 30.6 ms is used for each frame in all experiments. The code for the entering and exiting is essentially the same for all the sorting experiments. The procedure for identifying and sorting the individual mutants is discussed separately and in greater detail.

Waiting for Worm to Enter:

The procedure for loading a worm is identical regardless of the genotype and whether the screen is done at high or low magnification. The valve that controls the side channels is opened to allow flow through the channel, while all the other valves are closed. Frames from the camera are continually grabbed and analyzed to determine the presence of an animal by the average pixel intensity over a threshold.

Waiting for a Worm to Exit:

Once the decision has been made as to where the animal should exit, the valve that controls that channel is opened as well as the L-shaped positioning valve to expedite exiting. During this time, frames from the camera are continually acquired, and once no animal is detected to be present in the channel, the exit channels and the L-shaped positioning valves are closed immediately while the side channels are opened. For high magnification (e.g. 100x) sorting, only a fraction of the field of view is visible. In order to ensure that an animal has completely exited the imaging zone, a 300-ms delay is added to the routine before closing the exit channels.

Image Processing and Decision Making

Automated Imaging and Identification of AQR and PQR

The image acquisition process for CX6858 was as described in the article. To analyze the images, out-of-focus frames were discarded and the images are convolved with a matrix to accentuate small bright regions. A threshold was applied to determine the fluorescence from the intestine as well as AQR and PQR. Different thresholds are then applied to the left and right nematode centroid to identify AQR and PQR and to distinguish PQR from the intestine auto-fluorescence. Groups of remaining pixels are then compared based on a number of features (size, position, etc) to determine whether AQR and PQR are present, and if so, where they are located. The correctness of the output for each animal was independently verified. Comparisons between manual and automated imaging and classification of different batches of animals showed a high degree of similarity (**Fig. 3n** and **Supplementary Fig. 7**).

Cellular Imaging of AWC Neurons

To locate the AWC neurons, sparse z-stacks (5-μm steps) are gathered along the A-P axis of the worm. It takes < 10 seconds to image an entire L4 animal at 100x using a 5 μm step size. These z-stacks are then flattened by computing the standard deviation of pixel in the x-y plane along the z-direction. To ensure that intestine autofluorescence is not

mistakenly identified as a neuron, intestine fluorescence is located and removed from the picture. A threshold is applied to this newly flattened image and the neuron(s) are located. The xyz stage then moves to the location of the neuron(s) to grab a more detailed z-stack (1 μm step size) which is necessary to determine whether one or two AWC-ON neurons are present. This z-stack is similarly flattened and a threshold is applied to determine the number of neurons.

Subcellular Imaging of CZ5261 and CZ5264

The sorting of strains CZ5261 and CZ5264 relies on determining the locations of GFP along the nerve cord. This is done using the same methods as mentioned earlier, namely compressing the z-stack to the x-y plane and then convolving it with a matrix to accentuate the puncta. A threshold is subsequently applied to the image to locate the puncta and depending on the number of puncta present and other features, the animals are determined to be either wild-type or have an *unc-16*$^{-/-}$ background.

7. Sorting Wild-Type and Mutant Classes

The work in this paper focuses on the sorting of wild-type animals from previously determined mutants based on a decision boundary created by classifying both populations using a variety of features (morphological and not). To do this we selected a number of features of potential interest that might provide information on differences between the mutant and wild-type populations. Some of these selected features are shown (**Supplementary Fig. 5a)**. A few features are illustrated that largely capture the differences between the two classes (**Supplementary Fig. 5b)**. With this information, it was relatively easy to create a decision boundary for classifying and sorting. Furthermore, with our system, future end-users may wish to identify animals of previously unknown phenotypes differing in some way from the wild-type population, for example in forward genetic screens. In this case, the wild-type population could be modeled using the similar feature space, and any animals significantly different from this population would be identified and collected.

8. Characterization of temperature distribution in the detection zone by numerical simulation

It is currently technically not feasible to measure the exact temperature that the animals experience at the detection zone noninstrusively. We did, however, measure the temperature of the coolant coming into the device as well as leaving the device, in addition to the temperature of the chip on the PDMS side and on the glass side. To characterize the temperature distribution inside the chip, we use numerical simulations coupled with boundary conditions from experimentally measured values and physical parameters of the materials and fluids used in the experiments.

The simulations of the coolant flow and heat transport in the device were performed using a commercial finite element package COMSOL (Stockholm, Sweden). The actual three-dimensional geometry of the section of the device is shown (**Supplementary Fig. 3a)**. To simulate coolant flow in the temperature control channel, the incompressible steady-state Navier-Stokes equations were used. The pressure at the outlet was fixed at

atmospheric pressure and the fluid velocity at the inlet was set at the parabolic flow profile with the volumetric flow rate as measured. To simulate heat transport numerically, the convection-conduction equation was used. To reduce the number of mesh elements, the thermal conductivity of upper part of the PDMS and the actual geometry were rescaled by the equation, $k_{PDMS}/L_{PDMS} = k'_{PDMS}/L'_{PDMS}$. The temperature of the coolant at the inlet was fixed at 260 K as measured experimentally with a thermocouple. The temperature of the surface of the cover glass was also fixed at 286 K as measured. The temperature fields at the various cross-sections shown in **Supplementary Figure 3b** confirms localized cooling. Inset of **Supplementary Figure 3b** shows temperature profile at the vertical mid-plane of the detection zone. Based on this model, the average temperature in the detection zone was found to be around 4°C.

References

1. Jackman, R.J., Duffy, D.C., Cherniavskaya, O. & Whitesides, G.M. Using elastomeric membranes as dry resists and for dry lift-off. *Langmuir* **15**, 2973-2984 (1999).
2. Brenner, S. Genetics of Caenorhabditis-Elegans. *Genetics* **77**, 71-94 (1974).